

Executive Summary

Using Rensselaer Polytechnic Institute's (RPI's) wind tunnel located in the Johnson Engineering Center (JEC), measurements of the aerodynamic forces on a Stingray Unmanned Aerial Vehicle (UAV) were taken using a 6-component sting balance were used and used to observe the effects that flaps have on the lift, drag, and pitching moment of an aircraft. When using a 6-component sting balance it is important to correct the indicated force and moment values for the aerodynamic center offset, but the Stingray UAV had an aerodynamic center offset of 0. These tests were run at Reynold numbers of 152,823 and the model used had a planform area of 0.306875 squared feet. Two different wingtip configurations were used, one with zero flap angle as a baseline and one with a 25 degree downward flap angle on both the right and left side of the model.

For the baseline wingtip configuration the zero-lift angle of attack is approximately at -2 degrees and the coefficient of lift reached a maximum of about 0.75 at 14 degrees without hitting stall. The coefficient of drag peaked at around 0.02 at -2 degrees. For the 25 degree downward flap configuration the zero-lift angle of attack had decreased to -4 degrees and the coefficient of lift reached a maximum of about 0.85 at 14 degrees, still without hitting stall. The coefficient of drag peaked at around 0.0375 at -2 degrees.

Flow visualization using helium bubbles provided qualitative insight into airflow behavior for both configurations, including a way to observe the streaklines and pathlines of the flow. For both configurations and at all angles of attack very minimal flow separation was observed as well as no vortices. This supports the quantitative data by showing that a larger angle of attack would be required to cause flow separation and reach stall. The minimal separation observed in the streaklines also aligned with the low values of drag seen in the data as well, showing that the Stingray UAV achieves its structural purpose of having high lift and low drag.

Introduction

On an aircraft, flaps play a critical role in both takeoff and landing. The main purpose of flaps is to increase both lift and drag by effectively increasing the camber of the airfoil and virtually increasing the angle of attack as highlighted in Figure 1 (Anderson, 2016). The degree to which lift and drag are increased is related to the angle of flaps relative to zero degrees, also called ‘no flaps’.

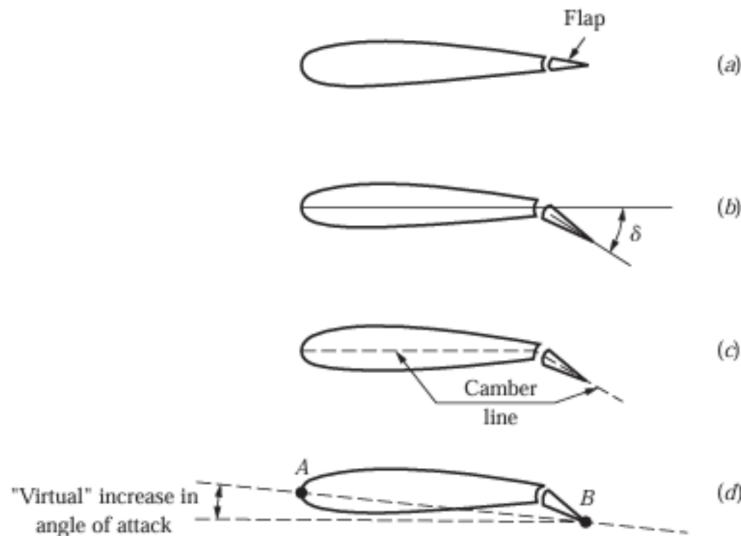


Figure 1: Visualization of the effects of flaps on airfoil characteristics (Anderson, 2016)

To better understand the effects of flaps on the key aerodynamic forces and moments, this experiment was performed with the purpose of measuring the aerodynamic lift, drag, and pitching moment of a Stingray Unmanned Aerial Vehicle (UAV) with no flaps (flap angled at zero degrees), and with flaps opened at a high angle. There is no equation for the effect of flaps on the aerodynamic forces and moment coefficients, and so comparisons will be made directly from the collected data. It is also important to visualize the qualitative characteristics of flow about the stingray, noting flow separation, the streamlines, lines tangent to the velocity profile of flow, pathlines, lines traced out by single particles traveling across the flow, and streaklines, lines connecting all particles that have crossed a particular point in space for a given range of time.

To characterize the flow, it is essential to note the properties of airflow to calculate the density

of air, kinematic viscosity and Reynolds number of flow. Air density, ρ , is calculated from the ideal gas law,

$$\rho = \frac{P_{static}}{RT} \quad (1)$$

where P_{static} is the ambient pressure, T is the tunnel temperature, and R is the specific gas constant of air, equal to 1716.6 pound force foot per slug degree Rankine ($\frac{lb_f * ft}{slug * ^\circ R}$). Kinematic viscosity, ν , is the ratio of dynamic viscosity, μ , to air density.

$$\nu = \frac{\mu}{\rho} \quad (2)$$

Dynamic viscosity is tabulated in literature (Mitchell, 2020). The Reynolds number quantizes the relative influence of inertial forces, based on the free-stream velocity, U , to viscous forces in fluid flow and roughly predicts the behavior of flow based on the scale of the system, determined by the characteristic length, which was defined as c , the mean chord length.

$$Re = \frac{Uc}{\nu} \quad (3)$$

For the first part of this experiment, a single free-stream velocity of 75 feet per second (fps) was used to collect data. At this velocity, the properties of air is not expected to deviate from standard values by a significant amount, and so the magnitude of the Reynolds number can be calculated from these values. A Reynolds number of about 200,000 was expected for this experiment, which assumes generally laminar flow. In laminar flow, the streamlines, pathlines, and streaklines are all coincident.

For the first part of the experiment, aerodynamic forces were collected using an NK Biotechnical Mini 6-Force sting balance which collected the indicated lift, L_i , and drag, D_i , in pounds of force (lb_f), and the indicated pitching moment, M_i , in inch pounds of force ($in * lb_f$). This in reference to the sting's position and thus the value of the pitching moment was offset by some distance from the aerodynamic center of the Stingray UAV model. To determine the values for

lift, drag, and moment about the aerodynamic center, the offset, x , and angle of attack, α , must be accounted for:

$$M = M_i - xL_i \quad (4)$$

$$L = L_i \cos(\alpha) - D_i \sin(\alpha) \quad (5)$$

$$D = D_i \cos(\alpha) - L_i \sin(\alpha) \quad (6)$$

The AC offset, x , for the Stingray UAV model is zero, so the indicated value of pitching moment from the sting balance will be equal to the final value at aerodynamic center.

The final values for lift, drag, and pitching moment can be non-dimensionalized using the planform area, S , of the Stingray UAV, chord length, and dynamic pressure, q .

$$S = \frac{1}{2}b\sqrt{a^2 - \frac{1}{4}b^2} \quad (7)$$

$$q = \frac{1}{2}\rho U^2 \quad (8)$$

The definitions of a and b in Equation 7 are shown in Figure 2.

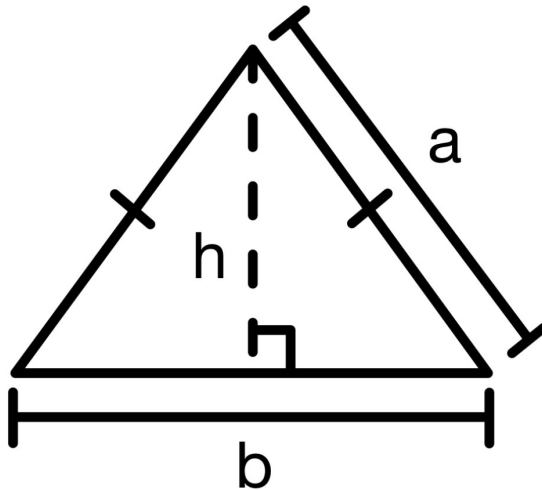


Figure 2: Simplified Geometry of the Stingray UAV planform area

The non-dimensional values of the aerodynamic forces and moments, or the lift, drag, and

pitching moment coefficients, are given in the following equations (Anderson, 2017).

$$C_L = \frac{L}{qS} \quad (9)$$

$$C_D = \frac{D}{qS} \quad (10)$$

$$C_M = \frac{M}{qSc} \quad (11)$$

These can be used to compare the lift, drag, and pitching moment between no flaps and high-angle flaps.

It can be useful to qualitatively observe the flow over the model as well, such as using helium bubbles to visualize the flow around the Stingray UAV model, similar to the photographs shown in Figure 3. Doing so better captures the physical behavior of airflow around the model and allows for comparisons of the flow around the tail end of the model as the flaps changed to connect the quantitative data collected with the physical phenomena caused by the flaps.

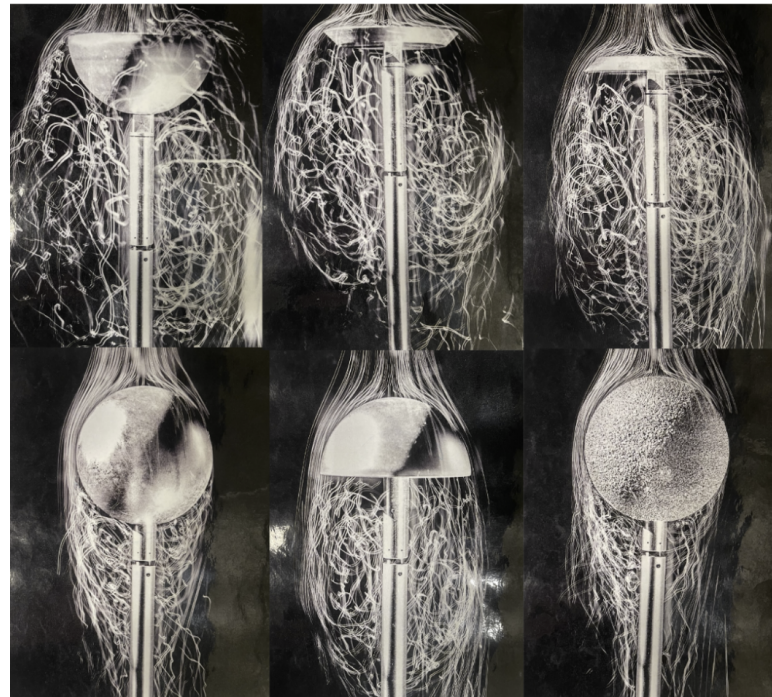


Figure 3: Helium bubbles visualizing flow over various bluff bodies

Experimental Setup

In this experiment, the objective was to investigate the aerodynamic performance of one of three given aircraft. The given aircraft models were the Cessna 182, T38 Trainer, and the Stingray UAV. Beside these set constraints, the setup and procedure was selected by the team, taking into consideration time and depth of data. Options for aerodynamic quantities to be measured include lift, drag, and side forces, along with the corresponding moments (pitch, roll, and yaw). The three chosen for this experiment were the lift, drag, and pitching moment. This data can then be used to compute non dimensional aerodynamic coefficients such as lift coefficient, drag coefficient, and pitching moment coefficient. At first, the Cessna model was selected, but due to an issue with the model, it was switched for the Stingray UAV, which features an approximate wingspan of 12 inches (in) and an average chord length of 4.125 in, as shown in Figure 4. Prior to testing, the model's geometry was measured using a tape measure with an accuracy of $\pm 0.5\%$ to confirm actual dimensions and verify the offset between the aerodynamic center and the balance center, ensuring that all measured forces and moments were correctly referenced.

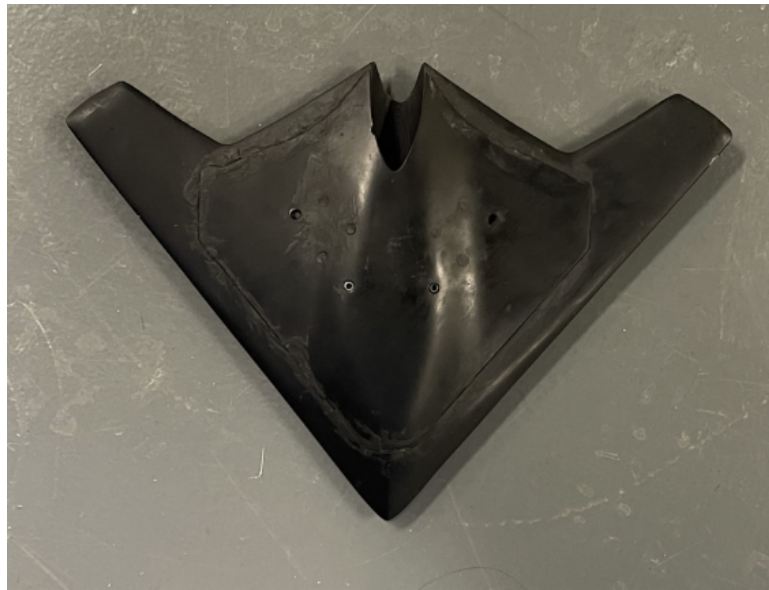


Figure 4: Stingray UAV model

Tests will be set at angles of attack of -4 degrees to 14 degrees with increments of 2 degrees (10 measurements) repeating with alternative wing tips. Measurements were taken with a Mini

6-component sting balance and the closed return wind tunnel at the Jonsson Engineering Center at Rensselaer Polytechnic Institute.

The coordinate system was defined such that the origin was located at the aerodynamic center, the X-axis extended downstream, the Z-axis pointed vertically upward, and the angle of attack, θ was defined as positive for nose-up configurations, as shown in Figure 5:

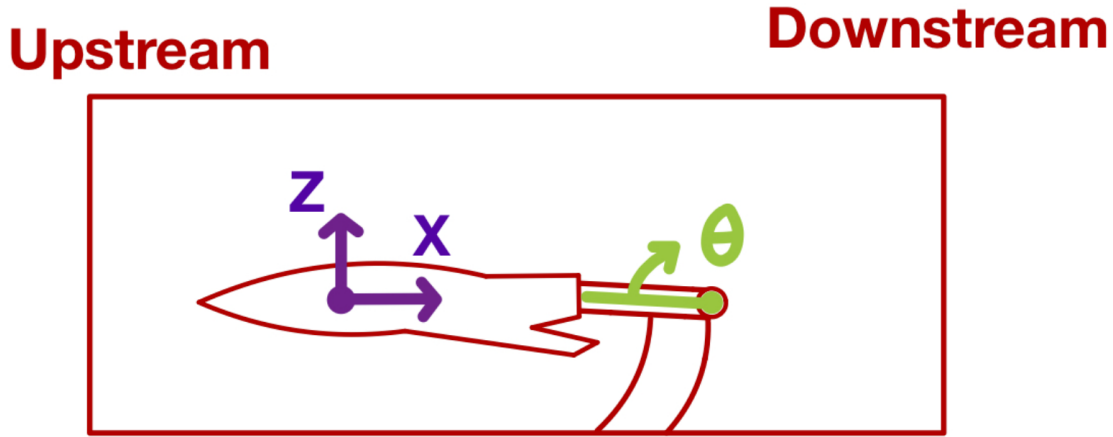


Figure 5: Coordinate system of Stingray UAV in the wind tunnel

The quantitative experiment began with the baseline configuration (flaps set to 0°). The wind tunnel speeds were set to 75 fps for the runs. At the tunnel speed, the angle of attack (AOA) was varied from -4° to 14° in 2-degree increments. At each AOA, the flow was allowed to stabilize before forces and moments were recorded using LabView VI. For each configuration, lift, drag, and side forces were measured, along with pitch, roll, and yaw moments. When this testing section concluded, it was repeated with the alternative wing tip of a 25° inner downward flap on both the left and right sides. To do this, the model was carefully removed from the sting balance and its top shell was removed in order to get full access to the wing tips. Afterward, the chosen alternative wingtips were installed. The baseline 0° wingtips and the alternative 25° wingtips can be seen in Figures 6 and 7 respectively.

Following the quantitative measurements, a qualitative flow visualization was performed using helium bubble flow tracing. The system was set up to release helium bubbles into the flow, enabling visualization of surface flow and separation regions. The model with the alternative wingtip



Figure 6: The baseline 0° wingtips



Figure 7: The alternative 25° wingtips

configuration was initially positioned at an AOA of 14° , then 0° , and lastly -4° as the wind tunnel speed was reduced to 10 fps for visualization clarity. Bubble patterns were observed and photographed before the process was repeated for baseline wingtip configuration. The helium bubble flow tracing system can be seen in Figure 8.



Figure 8: Helium Bubble flow tracing system

Results and Discussion

For this experiment, data was collected on the Stingray UAV in two different configurations. In the first configuration, which is considered the baseline configuration, the flaps were set at 0 degrees. In the second configuration, the 0-degree flaps were swapped out for 25-degree flaps angled downward. The force measurements from the sting were used to calculate the aerodynamic coefficients C_L , C_D , and C_M in these two configurations, while photos of helium bubbles in the wind tunnel were taken to qualitatively analyze the streaklines around the UAV in these configurations.

Experiment 6.1: Force Balance Measurements for Lift, Drag, and Pitch for Stingray UAV in Base Configuration and with Flaps Down

For the first part of this experiment, the forces on the Stingray were measured to calculate the lift, drag, and pitching moment. To conduct these calculations, the planform area of the Stingray had to be calculated. For simplicity, the planform area was idealized to be a triangle with a side length of 9.5 in \pm 0.015625 in, and a base of 12 in \pm 0.015625 in. Using Equation 7, the planform area was found to be 0.306875 ft². As for the Reynolds number, this was calculated using Equation 3 where the flow velocity is 75 fps, the dynamic viscosity is 1.687e-4 ft²/s, and the chord length is 0.34375 ft (Mitchell, 2020). This results in a Reynolds number of 152,823. Equations 5, 6, and 4 were used to correct the lift, drag, and pitching moment respectively for each angle of attack. The dynamic pressure was calculated for each data point using Equation 8. Equations 9, 10, and 11 were then used to calculate the coefficient of lift, drag, and pitching moment at each point.

For the baseline wingtip configuration the data was plotted in Figure 9. In Figure 9a it can be seen that the zero-lift angle of attack is approximately at -2 degrees and the C_L continues to climb with increasing angle of attack, reaching a maximum of about 0.75 at 14 degrees. The Stingray UAV is modeled to be a blended wing body wherein the entire craft acts as one large wing generating significant lift as the angle of attack increases (Ikeda and Bil, 2006). The C_L plot shows a continued linear increase and no stall is observed within the tested range. This shows that the stall angle for the baseline UAV configuration is greater than 14 degrees. This is much larger than it was for the airfoils in Experiment 4. In Figure 9b C_D is peaking at around 0.02 at -2 degrees but decreases to negative values beyond 4 degrees AoA. This negative drag makes sense due to the stingray UAV design to reduce drag as much as possible.

For the downward flap configuration the coefficient of lift, pitching moment, and drag were each plotted against the tested angles of attack in Figure 10a-c, while the coefficient of drag was plotted against the coefficient of lift in Figure 10d.

From observing Figure 10a, it can be seen that the zero-lift angle of attack has decreased to -4 degrees, but continues to increase with the angle of attack, like in the baseline configuration.

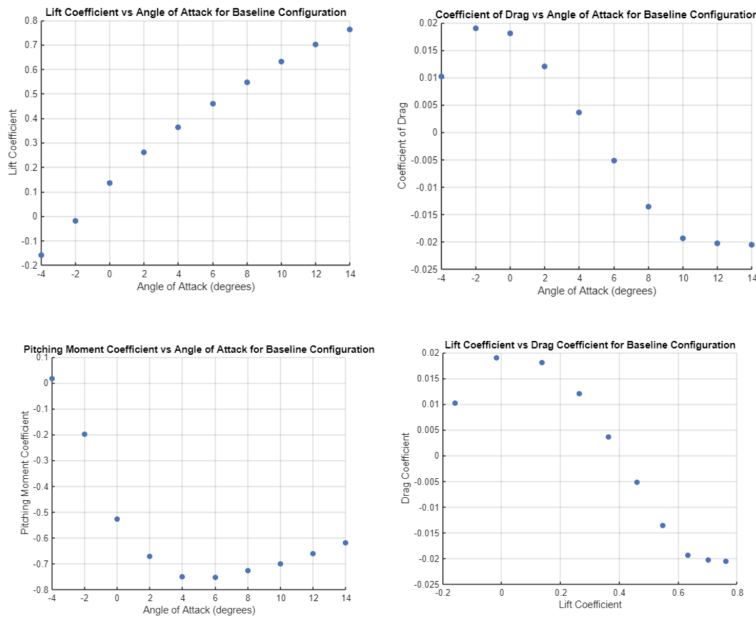


Figure 9: Stingray UAV test results for baseline condition. Subplots are labeled a-d reading from left to right like a book

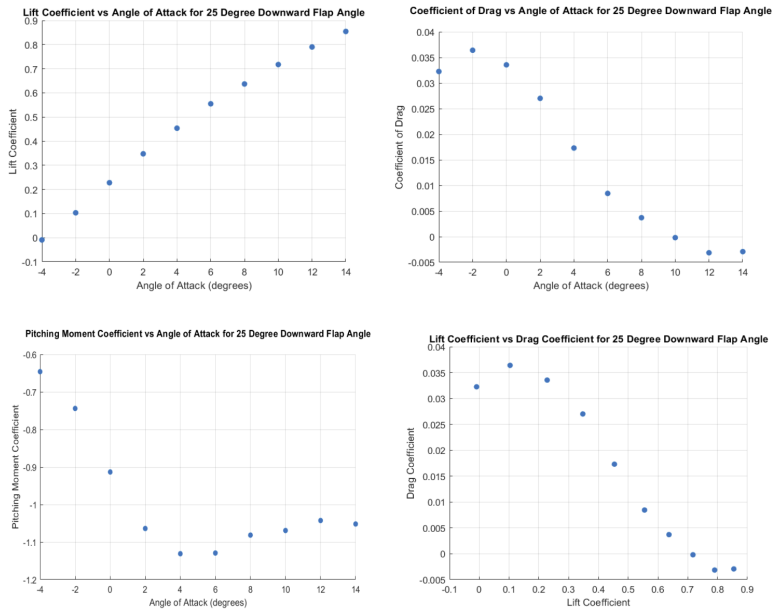


Figure 10: Stingray UAV test results for flap down condition. Subplots are labeled a-d reading from left to right like a book

This is likely once again due to the very nature of blended wing body aircraft and how they are built to be as aerodynamically efficient as possible, while the decreased zero angle of attack can be attributed to the flaps being downward (Ikeda and Bil, 2006). In Figure 10c, the pitching moment coefficient increases very quickly with angle of attack before stabilizing at a value of about -1.1. Now, Figure 10b seems to show that the coefficient of drag begins positive, but then decreases to zero, and even becomes negative with increasing angle of attack, which does not appear to make much physical sense. For most other cases, a greater angle of attack should increase the drag as well since the model becomes more like a bluff body, and experiences a greater pressure difference between its front and back. Thus, this effect may either be caused by some unknown error in the lab, by some other property of blended wing body designs, or perhaps even a drag crisis occurring. Finally, in Figure 10d, the coefficient of drag is nearly an order of magnitude smaller than the coefficient of lift and sharply decreases with an increasing coefficient of lift. Once again, this is possibly due to the blended wing body design, which is optimized to reduce drag (Ikeda and Bil, 2006).

These results are somewhat consistent with those found in other literature that tests other blended wing body craft. In a paper by Farnsworth, Vaccaro, and Amitay, which tests the exact model used in this experiment at a similar Reynolds number of 185,000, it was also found that the coefficient of lift continuously increased with angle of attack with no sign of stall occurring within the tested range of angles (Farnsworth et al., 2008). The pitching moment coefficient was also found to be fairly invariant with angle of attack beyond 0 degrees (Farnsworth et al., 2008). In another paper by Carter, Vicroy, and Patel, similar results were found for the coefficient of lift, though the coefficient of the pitching moment decreased and then increased instead of decreasing and then settling at a specific value (Carter et al., 2012). Though it should be noted that the specific aircraft tested in this paper differed a fair amount from the one used in this experiment.

Experiment 6.2 Helium Bubble Flow Visualization for Stingray UAV

To further investigate the flow behavior around the Stingray UAV helium bubble flow visualization was conducted at a wind tunnel speed of 10 fps. This allowed for the observation of streaklines around the model, providing insight into the flow behavior and potential separation points at various angles of attack. The resulting streaklines, shown in Figure 11, help to provide a visual understanding of flow dynamics over the blended wing body.

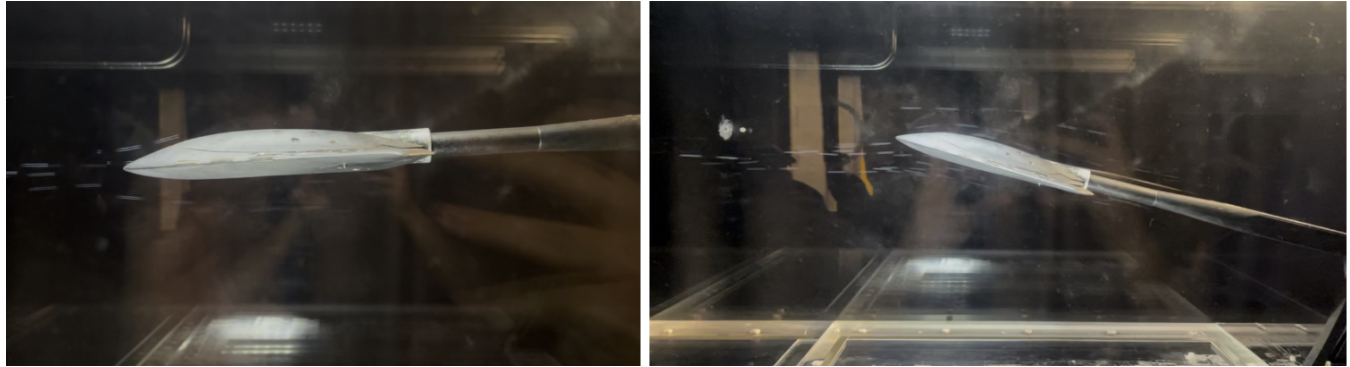


Figure 11: Helium Bubble flow for baseline wingtip configuration. 0 degrees angle of attack is shown on the left (a) and 14 degrees is shown on the right (b)

In Figure 11b at an AoA of 14 degrees the streaklines closely follow the contour of the Stingray model along the leading edge and upper surface indicating that the flow remains largely attached over the blended wing body. However near the trailing edge small vortices are visible as the streaklines begin to curve and disrupt suggesting the onset of flow separation due to the high angle of attack. Despite this, no significant separation occurs which aligns with the force balance measurements showing a high lift coefficient of 0.75 and no stall within the tested range. In Figure 11a, at 0 degrees angle of attack, the streaklines are smooth and follow the model's contour from the leading edge to the trailing edge with no visible vortices indicating fully attached flow. These streaklines reinforce the conclusion that the stall angle for the baseline configuration is greater than 14 degrees, supporting the findings from the quantitative data.

Streaklines were also captured for the 25-degree downward wingtip configuration using helium bubbles for angles of attack at -4, 0, and 14 degrees, which are shown in Figures 12, 13, and 14 respectively.



Figure 12: Helium Bubble flow for flap down wingtip configuration at Angle of Attack of -4 Degrees



Figure 13: Helium Bubble flow for flap down wingtip configuration at Angle of Attack of 0 Degrees



Figure 14: Helium Bubble flow for flap down wingtip configuration at Angle of Attack of 14 Degrees

In both Figures 12 and 13, the streaklines are fairly smooth and follow the curve of the Stingray model, with only small vortices generated in the very back where the flap is angled downward. In Figure 14 the higher angle of attack appears to generate slightly larger vortices, though the helium bubble streaklines still follow the model very closely, again indicating that flow separation has yet to occur and further reinforcing the idea that the model's stall angle, even with the downward flaps, is greater than 14 degrees.

Conclusion

This concludes the experiment.

References

- Anderson, J. D., *Introduction to Flight*, 8th ed., McGraw-Hill Education, 2016.
- Mitchell, J. W., *Introduction to Fluid Mechanics*, 10th ed., John Wiley Sons, 2020.
- Anderson, J. D., *Fundamentals of Aerodynamics*, 6th ed., McGraw-Hill Education, 2017.
- Ikeda, T., and Bil, C., “Aerodynamic Performance Of A BlendedWing-Body Cconfiguration Aircraft,” , 2006. URL https://www.icas.org/icas_archive/ICAS2006/PAPERS/304.PDF.
- Farnsworth, J. A. N., Vaccaro, J. C., and Amitay, M., “Active Flow Control at Low Angles of Attack: Stingray Unmanned Aerial Vehicle,” , 2008. URL <https://arc.aiaa.org/doi/pdfplus/10.2514/1.35860>.
- Carter, M. B., Vicroy, D. D., and Patel, D., “Blended-Wing-Body Transonic Aerodynamics: Summary of Ground Tests and Sample Results,” , 2012. URL <https://ntrs.nasa.gov/api/citations/20090007702/downloads/20090007702.pdf>.

Appendix A: MATLAB Code used to Plot Graphs for Experiment 6.1

```
clc;
clear;
close all

opts = delimitedTextImportOptions("NumVariables", 8);

% Specify range and delimiter
opts.DataLines = [5, Inf];
opts.Delimiter = ",";

% Specify column names and types
opts.VariableNames = ["alphadeg", "Lift", "Drag", "Side", ...
    "Pitchin", "Yaw", "Roll", "Velocityfps", "TemperatureF", "AtmPressuremillibars", "VarName8"];
opts.VariableTypes = ["double", "double", "double", ...
    "double", "double", "double", "double", "double", "double", "string"];

% Specify file level properties
opts.ExtraColumnsRule = "ignore";
opts.EmptyLineRule = "read";

% Specify variable properties
opts = setvaropts(opts, "VarName8", "WhitespaceRule", "preserve");
opts = setvaropts(opts, "VarName8", "EmptyFieldRule", "auto");

% Import the data
Lab6 = readtable("C:\Users\tomor\Downloads\goyzueta-lab-6.csv", opts)
```

```

AoA=Lab6(14:23,1);
Lift=Lab6(14:23,2);
Drag=Lab6(14:23,3);
PM=Lab6(14:23,5);
Vel=Lab6(14:23,8); %fps
Temp=Lab6(14:23,9); %F
Pstat=Lab6(14:23,10); %mbar

AoA = table2array(AoA)*(pi/180);
Lift = table2array(Lift);
Drag = table2array(Drag);
PM = table2array(PM);
Vel = table2array(Vel);
Temp = table2array(Temp)+460; %R
Pstat = table2array(Pstat)*2.088546; %psf

c=4.125/12 %ft
S=0.306875 %ft^2
R=53.35 %lbf*ft/(lbm*R)
q=Vel.^2.*2.284e-3.*0.5 %psf

Cl=Lift./(q.*S)
Cd=Drag./(q.*S)
Cm=PM./(q.*S.*c)

```

```

AoA=AoA*(180/pi)
scatter(AoA,Cl,'filled')
title('Lift Coefficient vs Angle of Attack for 25 Degree Downward Flap Angle')
xlabel('Angle of Attack (degrees)')
ylabel('Lift Coefficient')
grid on
scatter(Cl,Cd,'filled')
title('Lift Coefficient vs Drag Coefficient for 25 Degree Downward Flap Angle')
xlabel('Lift Coefficient')
ylabel('Drag Coefficient')
grid on
scatter(AoA,Cm,'filled')
title("Pitching Moment Coefficient vs Angle of Attack for 25 Degree Downward Flap Angle"+newline)
xlabel('Angle of Attack (degrees)')
ylabel('Pitching Moment Coefficient')
grid on
scatter(AoA,Cd,'filled')
title("Coefficient of Drag vs Angle of Attack for 25 Degree Downward Flap Angle"+newline)
xlabel('Angle of Attack (degrees)')
ylabel('Coefficient of Drag')
grid on

```